Conductivity study of Zeolitic Imidazolate Frameworks, Tetrabutylammonium hydroxide doped with Zeolitic Imidazolate Frameworks, and mixed matrix membranes of Polyetherimide/Tetrabutylammonium hydroxide doped with Zeolitic Imidazolate Frameworks for proton conducting applications

J. Vega[a]

A. Andrio[b]

A.A. Lemus[a]

L.F. del Castillo[c]

V. Compañ[d, *]

vicommo@ter.upv.es

[a]Centro de Investigación en Ciencia Aplicada y Tecnología Avanzada, Unidad Legaría, Instituto Politécnico Nacional, Legaria Núm. 694, Col. Irrigación, Miguel Hidalgo, C.P. 11500 Cd, Mexico

[b]Departamento de Física aplicada, Universitat Jaume I, 12080, Castellón, Spain

[c]Departamento de Polímeros, Instituto de Investigaciones en Materiales, Universidad Nacional Autónoma de México (UNAM), Ciudad Universitaria, Apartado Postal 70-360, Coyoacán, 04510, Mexico

[d]Departamento de Termodinámica Aplicada, Escuela Técnica Superior de Ingenieros Industriales (ETSII), Universidad Politécnica de Valencia, Campus de Vera s/n, 46020, Valencia, Spain

*Corresponding author.

Abstract

ZIF-8 (Z8), ZIF-67 (Z67), and ZMix, a Zn/Co bimetallic zeolitic imidazolate framework (ZIF), were synthesized and doped with tetrabutylammonium hydroxide (ZIFsT). The obtained powders were used as fillers for polyetherimide (PEI) at a concentration of 20 wt %. The presence of the three ZIFsT in the polymeric matrix enhanced proton transport relative to that observed for PEI or ZIFs alone. The real and imaginary parts of the complex conductivity were obtained for each of the six materials, and the temperature and frequency dependence of the real part was analyzed. The results at different temperatures show that the dc-conductivity are about three orders of magnitude higher for the doped ZIFsT materials than for the PEI/ZIFsT membranes. In addition, the conductivity of the PEI/ZIFsT membranes increases five or six times when the temperature is changed from 25 °C to 55 °C. For these materials, the conductivity measurements have a linear dependency with frequency, which allowed for the creation of a master curve. It was also found that the PEI/ZMixT membrane activation energy is four times smaller than that of PEI/Z8T membranes and five times smaller than that of PEI/Z67T. Similarly, the real and imaginary parts of the complex dielectric constant were obtained, and the tan δ was evaluated. Using this value, the diffusion coefficient and the charge carrier density were obtained. A discussion of the proton transport mechanism through the membrane is given, and a comparison of this work with those on similar electrolyte membranes is included.

Keywords: Zeolitic Imidazolate Frameworks; Mixed Matrix Membranes; conductivity; PEI/ZIFsT membranes

1 Introduction

Currently, proton exchange membrane fuel cells (PEMFC) are the focus of attention in the development of electrochemical devices called fuel cells. These devices, which are capable of transforming chemical energy into electrical energy, have shown high performance in the conversion of energy from fuels such as hydrogen and methanol [1]. The operation of a PEMFC is similar to that of a galvanic cell where the electrons produced travel through an external circuit while the protons are transported through a barrier called a proton exchange membrane (PEM) which, in turn, prevents the passage of electrons and fuel [2]. Today, the most popular materials for PEMs are the perfluorosulphonic materials, among which the most outstanding is Nafion®. This is because the Nafion exhibits excellent mechanical properties, chemical stability, and high proton conductivity; however, its high cost and low operating temperature for proton transport are factors that influence the search for new proton conductive materials [3,4]. Sulfonation of polymers to produce, for example, sulfonated poly-ether-ether-ketone (SPEEK) seems to be a promising solution for the substitution of perfluorosulphonic materials because it has a proton conduction on the order of 10^{-2} S cm^{-1} (above 80 °C), which is similar to the that of Nafion membranes [5]. However, the degree of sulfonation of

SPEEK is closely linked to the degree of dissolution of the polymer in polar environments, which represents a considerable disadvantage [6,7]. Our group has reported SPEEK composite membranes with polyvinyl alcohol nanofibers (SPEEK/PVA) which exhibited mechanical stability in boiling water, acceptable proton conductivities, and excessive methanol permeabilities [8]. Other researchers have prepared ZrO_2/PEEK composite membranes (with an 87% degree of sulfonation) which resulted in a reduction of the methanol flow (60 times) but also a reduction of the protonic conductivity (13 times) [9]. As demonstrated, the synergy between the polymer and inorganic components can dominate the properties of the same materials when they are studied individually. Thus, the tunable properties of the polymer base are not the only ones that play an important role. The modification of the properties of the fillers may play a new important role. For example, Sadakiyo et al. [10], have reported on the dependence of the proton conductivity of MOF-$(NH_4)_2$ (adipic acid) [Zn_2(oxalate)$_3$] on the number of water molecules present in the framework, where the non-hydrated sample had a very low conductivity whereas the dihydrate and trihydrate samples exhibited conductivities of 7×10^{-5} S cm^{-1} and 8×10^{-3} S cm^{-1}, respectively.

The high microporosity and cavity volumes volume of the cavities of the zeolitic imidazolate frameworks (ZIFs) are factors of interest for the inclusion of guest molecules that favor protonic conduction through the framework. For example, Sadakiyo and co-workers [11] have reported that the inclusion of guest molecules in ZIF-8 increased the conductivity from 10^{-12} S cm^{-1} to 10^{-8} S cm^{-1} at 25 °C and 99% relative humidity (RH). This intrinsic property of ZIFs ensures that these materials will have high specific chemical reactivity, flexibility, and processability to make membranes oriented toward protonic transport with huge potential for energy applications.

In this work, the ionic pair of tetrabutylammonium hydroxide was introduced within the ZIFs in question, (ZIF-8 (Z8), ZIF-67 (Z67), and a Zn/Co bimetallic ZIF (ZMix)). Membranes which were resistant to wet conditions were prepared using the modified ZIFs (ZIFsT) as fillers into the polymer base polyetherimide (PEI), forming a mixed matrix membrane (MMM), PEI/ZIFsT. Our study focused on the protonic conductivities of the ZIFsT and PEI/ZIFsT (PZIFsT) membranes. It is believed that both vehicular transport mechanisms and Grotthuss contribute to the proton conductivity in MMMs, while the transport mechanism that predominates in the ZIFsT is Grotthuss. When the membrane is in humid conditions, the transport of protons is carried out at high frequencies, whereas when the membrane is dried or has a low degree of hydration, the transport is given at moderate and low frequencies.

2 Experimental

2.1 Chemical reagents

Tetrabutylammonium hydroxide (TBAH, 1.0 M); N-methyl-2-pyrrolidone (NMP, ≥99.7%; 2-methylimidazole (2-mIm, 99%); and zinc chloride ($ZnCl_2$, ≥97%) were purchased from Sigma Aldrich. Cobalt chloride ($CoCl_2$, ≥99.8%) and sodium formate (HCO_2Na, ≥99%) were purchased from Baker Analyzed and Reasol respectively.

2.2 Synthesis of ZIFs (Z8, Z67, and ZMix)

2.2.1 Z8 (ZIF-8)

Z8 was synthesized according to the reported procedure by McCarthy and co-workers [12]. In brief, 0.82 g of 2-mIm and 0.76 g of sodium formate were dissolved in 30 ml of methanol and then mixed with a 0.26 M $ZnCl_2$ methanolic solution. The obtained product was washed, centrifuged, and dried under vacuum for 12 h.

2.2.2 Z67 and ZMix (ZIF-67 and ZIF-Mix)

For the synthesis of Z67, 0.48 g of $CoCl_2$ was used in a similar procedure as for Z8. In the case of ZMix, a binary mixture of zinc and cobalt metal chlorides (Zn/Co: 0.17 g and 0.16 g respectively) was employed for promoting a solid solution with a 1:1 metal ratio.

2.2.3 ZIFsT (Z8T, Z67T, and ZMixT)

The ZIFs were added to the same solution of 3.5 ml of TBAH in methanol using 0.5 g of the appropiate ZIF was added to. The mixture was stirred for 12 h and placed in an ultrasonic bath for 30 min. The obtained products, ZIFsT, were collected by centrifugation, washed with deionized water, and dried under vacuum at 30 °C.

2.3 PZIFs and PZIFsT Mixed Matrix Membranes (PEI/ZIFs and PEI/ZIFsT)

2.3.1 PZIFs, PZIFsT

PEI was dissolved in an NMP solvent 1:3 (wt%) to form a colloidal solution to which ZIFs and ZIFsT powders were added 20 (wt%) (See Eq. (1)). To disperse the powders, the mixture flasks were sealed and placed in an ultrasonic bath for 1 hour. The following casting technique was used to prepare the films: the colloidal dispersions were spread on a flat glass and then placed in an oven to reach 100 °C at a heating rate of 20 °C/h. Once the set temperature was reached, the films were kept at this temperature for 12 h. The obtained membranes (with approximately 60 microns in thickness) were stored and sealed until further use. Acronyms for each membrane are used from now on: PZ8, PZ67, and PZMix are used for PEI/ZIFs membranes and PZ8T,

PZ67T, and PZMixT are used for the PEI/TBAH doped ZIFs membranes.

$$\%\ weight\ ZIF = \frac{weight\ \mathrm{ZIF}}{weight\ \mathrm{ZIF} + weight\ \mathrm{PEI}} \times 100\% \quad (1)$$

2.4 Scanning electron microscopy (SEM) study

The surface morphology of the samples: fillers (ZIFs) and membranes (PZIFs and PZIFsT) was investigated using a field scanning electron microscope (JEOL 7001F EDX-WDX Oxford, INCA 350/Wave 200). The samples were gold coated and conserved before SEM observations.

2.5 Thermogravimetric analysis

The thermal stability of the membranes was evaluated using a thermogravimetric analyzer from TA Instruments (model 2950). The temperature range for the analysis was 25 to 500 °C for fillers and 700 °C for PZIFsT with a heating rate of 5 °C/min. The experiments were carried out under nitrogen atmosphere using a flux of 60 ml/min.

2.6 Infrared spectroscopy (FTIR)

Fourier transform infrared spectroscopy (FTIR) spectra were measured at 25 °C using a Perkin-Elmer spectrophotometer equipped with a CsI beam splitter between 3500 cm^{-1} and 400 cm^{-1} For the determination of relative amounts of guest molecules in ZIFsT powders, KBr discs in a concentration of 0.1(wt%) of the corresponding ZIFsT were prepared. A 5 °C/min heating rate was used to reach the selected temperatures according to the observed TGA stages. Once the target temperature was reached, it was maintained for 5 min, and then the disc was analyzed by IR.

2.7 Porosity analysis

The material surface areas and the elemental composition of the samples (C, S, N) was determined using a sulfur and carbon elemental analyzer (Leco SC-144DR). N_2 adsorption isotherms were recorded at 77 K with an ASAP 2050 Pressure Sorption Analyzer (from Micrometrics) equipped with a Smart Vac degassing system. The processing of the adsorption data was carried to obtain the surface areas (BET and Langmuir) and the micropore volume. The sample was activated under vacuum at 100 °C for 2 hours before thermogravimetric analysis.

2.8 Impedance spectroscopy measurements

Impedance spectroscopy measurements were carried out on the ZIF fillers and PZIF membranes (PZ8, PZ67, and PZMix) with and without the incorporation of TBAH. Measurements were made within a 20–120 °C temperature range and within the frequency window of $10^{-1} < f < 3 \times 10^{6}$ Hz in dry and wet conditions in order to obtain the conductivity and diffusivity of the ionic charge carriers. The experiments were performed with a 100 mV amplitude using a Novocontrol broadband dielectric spectrometer (Hundsangen, Germany) integrated with an SR 830 lock-in amplifier with an Alpha dielectric interface. The sample of interest was sandwiched between two circular gold electrodes coupled to the impedance spectrometer, which acted as blocking electrodes. The membrane-electrode assembly was annealed in the Novocontrol setup under a dry nitrogen atmosphere prior to the start of the actual measurement. To guarantee the reproducibility of the measurement, the temperature was twice gradually raised and lowered from 20 °C to 120 °C in steps of 10 °C. At the third cycle of temperature scan, the dielectric spectra were collected at each step.

For the measurements in wet conditions, the samples were stored in bi-distilled water and subsequently sandwiched between the electrodes. During the measurements, the electrodes were kept in a BDS 1308 liquid device, which was coupled to the spectrometer and incorporated with deionized water to ensure that the sample was fully-hydrated below 100 °C and in equilibrium with its vapor above 100 °C, to simulate 100% RH atmosphere. For the isothermal experiments, the temperature was controlled by a nitrogen jet (QUATRO from Novocontrol) with a temperature error of 0.1 K during every individual sweep in frequency.

3 Results and discussion

3.1 Scanning electron microscopy analysis

For ZIFs, particle size is a critical factor in the properties and stability of the colloidal solution because smaller particles favor a better dispersion in the solution, and ultimately in the polymeric matrix upon the evaporation of the solvent. Additionally it is possible to achieve a larger effective contact area for transport carriers by using smaller particles. Fig. 1 shows SEM micrographs of the ZIF powders and the films obtained upon their incorporation into the PEI polymeric matrix. The average particle sizes obtained by SEM for Z8, Z67, and ZMix were 0.7, 0.5, and 0.2 μm, respectively. Initially, these sizes are quite similar to those already reported [12,13]. However, when during

preparation for casting (see the Experimental section), after one hour of ultrasonic bath the agglomerated crystallites break up, and diminishing their average size. Ultrasonic morphological modification is advantageous because, it promotes a larger effective contact area in the membrane due to the incorporation and distribution of smaller particles.

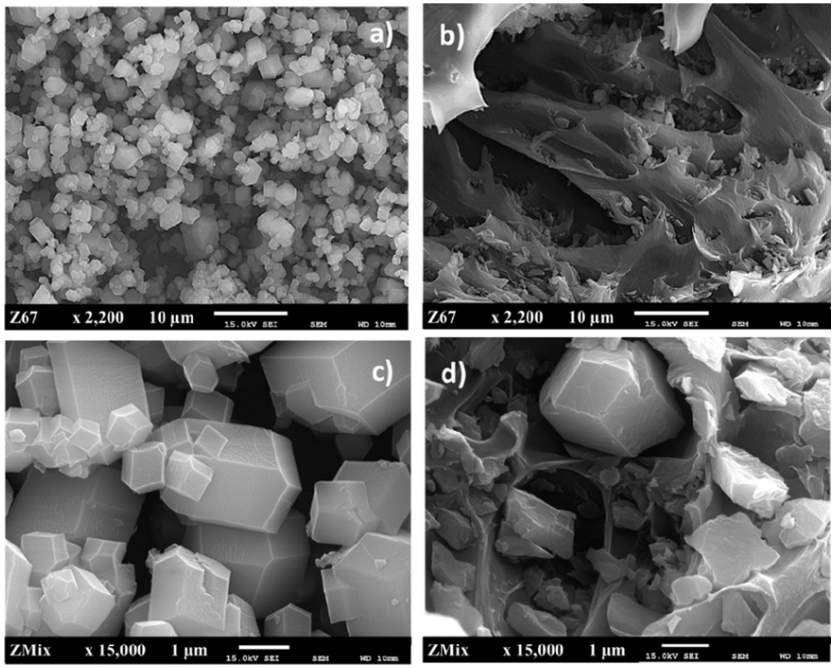

Fig. 1 SEM micrographs of powder materials a) Z67 and c) ZMix; within the PEI. b) PZ67 and d) PZMix, polymeric matrix.

alt-text: Fig. 1

3.2 Analysis of guest molecules in ZIFsT

Thermogravimetric studies were made for analyzing the thermal stabilities of ZIFsT powders and PEI/ZIFsT membranes. ZIFsT materials showed thermally defined stages for the guest molecules' evacuation; the first weight loss occurred from room temperature to approximately 120 °C. The most commonly evacuated molecule was water, however, it was present in slightly different amounts among the samples: 5.7% for Z8T and Z67T and 4.6% for ZMixT. In addition, the ZIFsT TGA curves provided information on the final-stage temperatures. Considering this, a thermal treatment was designed to correlate the weight losses observed in the thermograms with the IR-detected composition for the ZIFsT materials. Intensity changes in IR bands arising from the thermal treatment were used for semi-quantitative determination of TBAH content in each ZIFsT (see Fig. 2). The characteristic absorption band of the imidazole ring, which appears at 1140 cm^{-1}, was compared with the absorption band of the methylene group of TBAH, which appears at 2875 cm^{-1} [14]. It was assumed that there is no decomposition of the 2-methylimidazole ring in the analyzed temperature range, therefore, the 1140 cm^{-1} band was taken as a reference to calculate the relative concentration of methylene groups upon heat treatment.

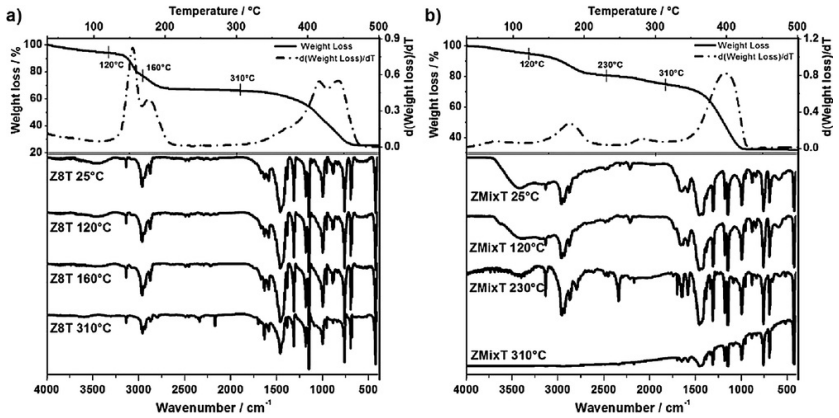

Fig. 2 Thermogravimetric analysis of samples a) Z8T and b) ZMixT (up) and the corresponding IR spectra after controlled thermal treatment (down) for the same materials.

alt-text: Fig. 2

The results are summarized in Table 1, where the relative TBAH concentration in ZMixT is more than twice the relative TBAH concentration in Z8T and Z67T.

Table 1 Relative concentration of guest molecules.

alt-text: Table 1

Sample	Temperature/°C	Absorbance/%[a]		Relative amount of guest molecules[c]
		Imidazole ring band ($(C_4H_5N_2)_2M$)[b])	Methylene group band (TBAH)	TBA Abs/12 CH_2 units
				($C_4H_5N_2$) Abs/24 rings in a cell unit
Z8T	25	81.6	20.1	0.49
	120	83.5	20.3	0.49
	150	85.3	20.5	0.48
	310	73	8.9	0.24
Z67T	25	81.6	21	0.51
	120	82.9	21.1	0.51
	230	84.8	21.4	0.50
	310	73.9	8.7	0.24
ZMixT	25	96	65	1.35
	120	97.7	62.4	1.28
	230	99.3	50.9	1.03
	310	99.7	–	–

[a] Absorbance values were used instead of transmittance values for ease of comparison. The absorbance of the imidazole ring was divided by the 24 rings present in the unit cell of the respective ZIF. The absorbance of the methylene group was divided by the 12 methylene units present in the tetrabutylammonium cation.

[b] $(C_4H_5N_2)_2M$, where M = Zn, Co, and Zn/Co is the empirical formula for each ZIF.

[c] A nondimensional value: % Absorbance/% Absorbance.

The difference found in water and TBAH content for each ZIFT is not dependent on the cavity size because they present in the same crystallographic phase and the difference in their cavity size is less than 1% [15–17]. Furthermore, the organic linker is the same in the three ZIFs studied. It contributes a hydrophobic character, which matches well with the aliphatic chains from the tetrabutylammonium cation. Nevertheless, this cation pairs with the hydroxide anion, and the presence of electrolytes change the environment of the cavity, which now has certain hydrophilic character [18]. No water crystallization amounts reported in the crystallographic information files highlight a notable difference in hydrophobic character for Z8 and Z67 (they indicate 10 and 2 water molecules, respectively) [16,17]; the TBAH doping process modifies the environment of the ZIFs and parallels the H_2O molecule content within the Z8T and Z67T frameworks. ZMixT on its own displays the highest TBAH content and is the only material that loses all methylene bands at 310 °C. This behavior exposes the existence of anisotropies in the electron charge distribution and in the resulting electric field for ZMix framework [12], which enhances the hydrophilic character of the cavity. This allows for better hosting of the electrolyte and a faster displacement of the ions from the framework at a specific temperature in comparison with Z8 and Z67.

After the guest molecules' removal, the TGA curves for ZIFsT exhibit the greatest weight loss related to the decomposition of the ZIF framework after 310 °C. In the TGA curve of the Z8T, a plateau appears from 200 °C to 310 °C and then the material exhibits a weight loss of 41.3%, which is related to the ZIF-8 decomposition. This behavior agrees with that previously reported [14]. The TGA curve of Z67T, on the other hand, shows a continued weight loss without a plateau after the removal of guest molecules (See Fig. S1 in the Supplementary Information). The decomposition of Z67 starts at 310 °C, which accounts for a mass loss of 33.8%. The ZMixT material shows a similar pattern of sustained weight loss once guest molecules leave, but the greatest loss starts at 320 °C and corresponds to a 41.8% weight loss, which is related to the ZMix decomposition (Fig. 2b).

In the case of the PEI/ZIFsT membranes, the three TGA curves present a similar behavior (a constant mass profile) from 300 °C until nearly 360 °C. The next mass loss of about 30% is in the 360–500 °C range. This final loss could be related to the decomposition of the ZIFs materials (see Fig. S2). From that point on, the curve follows a profile with a smooth slope which is likely related to the decomposition of the polymer base.

The decomposition temperatures of the ZIFsT structures determined in this work are low compared to those previously reported for ZIFs [14,15], demonstrating that TBAH doping affects the thermal stability of the microporous materials.

3.3 Porosity analysis

Fig. 3 shows the nitrogen sorption isotherms of the synthesized ZIFs and ZMixT. The results indicate a reversible type I isotherm, which is characteristic of microporous materials according to IUPAC [19]. As expected, the ZMix shows an intermediate sorption surface area value to the surface areas of Z8 and Z67 because ZMix has a 1:1 metal relationship. On the other hand, upon dedoping, the isotherm of ZMixT exhibits a surface area reduced by 27% in comparison with the ZMix sample.

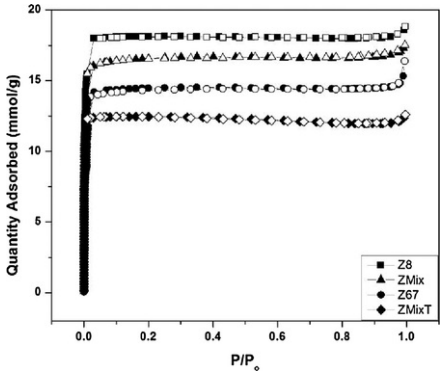

Fig. 3 N_2 adsorption/desorption isotherms at 77 K for ZIFs and ZMixT.

alt-text: Fig. 3

Table 2 shows the values obtained in nitrogen sorption/desorption study for the series of materials ZIFs and ZMixT.

Table 2 Textural properties of ZIFs and ZMixT materials obtained by nitrogen adsorption isotherms.

alt-text: Table 2

Sample	BET surface area ($m^2\ g^{-1}$)	Langmuir surface area ($m^2\ g^{-1}$)	Micropore volume ($cm^3\ g^{-1}$)
Z8	1279.4	1772.1	0.62
ZMix	1179.7	1634.3	0.53
Z67	1024.1	1420.1	0.48
ZMixT	857.9	1214.7	0.42

3.4 Impedance spectroscopy results

Impedance spectroscopy measurements were carried out on the fillers and mixed matrix membranes (MMM) in wet conditions (ZIFsTW and PZIFsTW) and dry conditions (ZIFsTD and PZIFsTD) at several temperatures in order to obtain the conductivity and diffusivity of ionic charge carriers. Both parameters characterize and estimate ionic transport in polymers and membranes. However, they are generally difficult to quantify. For comparison, we have also studied the permittivity of the fillers and MMMs. All the measurements have been done in dry and wet conditions to show that water molecules play an important role in creating the proton conducting pathways.

The experimental data obtained on the MMMs: PZIFsTW were analyzed in terms of the complex dielectric permittivity function, $\varepsilon^*(\omega,T)$, and the complex conductivity $\sigma^*(\omega,T) = j\ \omega\ \varepsilon_0\ \varepsilon^*(\omega,T)$ where j is the imaginary unity, ε_0 is the vacuum permittivity and ω the angular frequency of the applied electric field ($\omega = 2\pi f$).

Using dielectric spectroscopy measurements, the conductivities (σ_{dc}) were obtained from the Bode diagrams in the range of temperatures from 25 °C to 115 °C. Fig. 4 shows the Bode diagram for the real portion of the conductivity of the fillers, Z8TW (Fig. 4a), Z67TW (Fig. 4b), and ZMixTW (Fig. 4c), respectively.

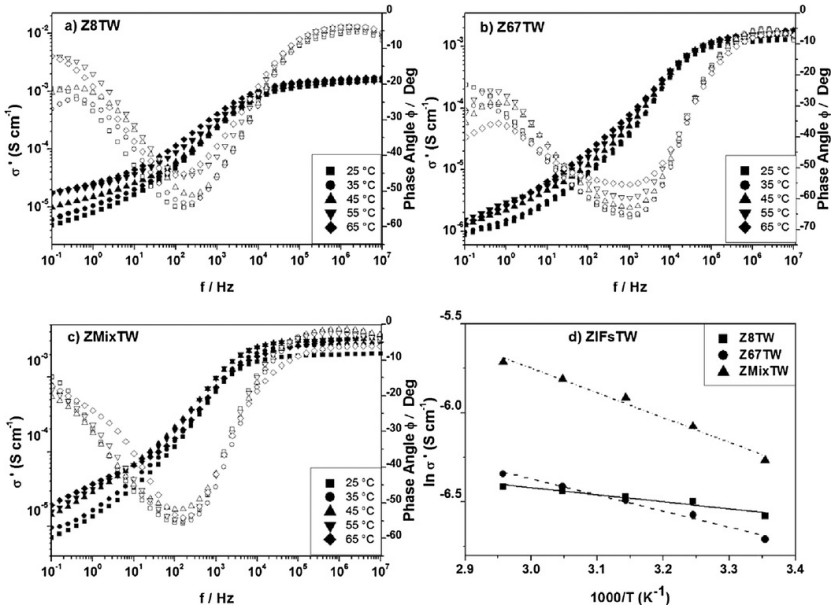

Fig. 4 Bode diagrams for the samples: a) Z8TW, b) Z67TW, c) ZMixTW in the range of temperature between 25 and 65 °C. d) Arrhenius plot for the conductivity of the ZIFsTW.

alt-text: Fig. 4

Notice that we have also plotted the phase angle in this plot to determine where it tended toward a zero value, in which case, the real part of the conductivity is independent of the frequency, such as that shown by the plateau.

This figure reveals that the real part of the conductivity increases with the frequency and tends to be a constant value when the phase angle (φ) reaches a maximum for each temperature. The dc-conductivity of the different ZIFs(σ_{dc}) can be extracted from the plateau in the high frequency range. Furthermore, the frequency value where the plateau is reached is shifted to the higher frequencies by increasing of the temperature as a consequence of the thermal activation of proton transport. However, at moderate and low frequencies, the conductivity decreases from σ_{dc}. The deviation from the plateau is attributed to the electrode polarization resistance which results from the blocking of charge carriers at the electrodes [20,21].

From the results shown from the Bode diagrams in Fig. 4, we can see that thermal activation is stronger for the ZMixTW than the singles (Z8TW and Z67TW). The comparison between the different ZIFsTW show that ZMixTW has a conductivity at 25 and 55 °C of 1.5×10^{-3} S cm^{-1} and 2.7×10^{-3} S cm^{-1}, respectively. These values are higher than the conductivity of Z8TW (1.0×10^{-3} S cm^{-1} and 1.46×10^{-3} S cm^{-1}, respectively) and Z67TW (1×10^{-3} S cm^{-1} and 1.50×10^{-3} S cm^{-1}, respectively).

The conductivity of the ZIFsT is proportional to the concentration of charge carriers (protons) present in the frameworks. Each ZIFT concentrates a different number of charge carriers due to the hydrophilicity of the cavity as a consequence of the inclusion of the organic salt TBAH. The greater hydrophilic character of the Z8T and Z67T cavities facilitates the access of water molecules to both the occupied and unoccupied cavities due to migration of hydroxide (OH^-) ions [11,22]. In addition to the hydrophilic character of the cavity of ZMixT, the local anisotropic electric field should be considered to explain the increase in the concentration of charge carriers and the better conductivity of ZMixT. The saturated experimental condition under which the conductivity analyses are carried out is the source of the increase in charge carriers.

The conductivity values increased with the temperature following the trend σ (ZMixTW) > σ (Z67TW) > σ (Z8TW). For example, at 25 °C, the values of the conductivities were 1×10^{-3} S cm^{-1}, 1.1×10^{-3} S cm^{-1} and 1.5×10^{-3} S cm^{-1} for Z8TW, Z67TW, and ZMixTW, respectively. In Fig. 4d, we represent the activation plot for the ionic conductivity as a function of temperature for Z8TW, Z67TW, and ZMixTW. In this figure, we observe Arrhenius behavior for all the ZIFsT. The apparent activation energies values obtained follow the tendency E_{ac} (Z67TW) = 8.3 ± 0.3 kJ/mol or 0.090 ± 0.003 eV < E_{ac}(Z8TW) = 11.1 ± 2.6 kJ/mol or 0.11 ± 0.03 eV < E_{ac} (ZMixTW) = 12.7 ± 0.5 kJ/mol or 0.130 ± 0.005 eV. These values are lower than those found for the activation energy for the conductivity of MOF-based proton conductors [22].

In Fig. 5, we can see the real part of the conductivity of the mixed matrix membranes PZ8TW, PZ67TW, and PZMixTW. From this figure, we observe a behavior quite similar to that observed for the fillers, which is also characterized by a plateau at moderate frequencies which correspond to the dc-conductivity, but with an important difference: there is a stronger temperature-dependence than in the fillers, where the curves were more compacted. Another difference is the existence of an angular frequency, ω_c, at which dispersion sets in and transitions into a power law at high frequencies. This behavior was not observed for the ZIFsTW in Fig. 4a–c, where the plateau was prolonged into the range of high frequencies.

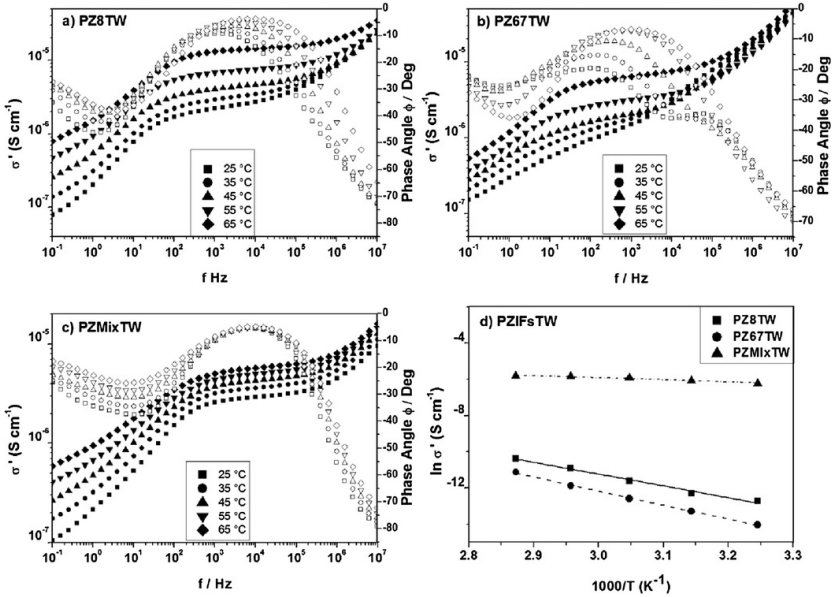

Fig. 5 Bode diagrams for the PZIFsTW samples a) PZ8TW, b) PZ67TW, and c) PZMixTW in the range of temperature between 25 and 65 °C. d) Arrhenius plot of conductivity as a function of inverse temperature of PZIFsTW.

alt-text: Fig. 5

When the ZIFsT are incorporated to the polymer matrix of PEI, we observe that the conductivity diminishes by about 3 orders of magnitude. However, the MMMs have a stronger dependence with temperature than ZIFsTW powder. A comparison with the behavior of the same samples in dry conditions (see Fig. S3 in the Supplementary Information) permitted us to observe the high dependence on wet conditions (about 95% humidity), where the values of conductivity obtained are about 3 or 4 orders of magnitude higher than those found in dry conditions. Similar results have been observed by other researchers in anhydrous proton-conducting MOFs, for which the proton conductivity at room temperature was found to be in the range of 10^{-8}–10^{-10} S cm^{-1} for Im@14 and Im@15 [23,24]. When the temperature was increased, an enhancement of the conductivity of about 3 orders of magnitude was also observed.

A comparison between Figs. 4 and 5 exhibits that the dielectric spectra of both ZIFsTW and polymerized ZIFsTW (PZIFsTW) forming the MMMs show that the values of the dc-conductivity are higher (around 3 orders of magnitude) for the ZIF materials than of the mixture of fillers with PEI. Similar results have been observed when the conductivity of Ils and polymerized ILs (PILs) were compared [25]. For example, at 25 °C, the conductivities values are 1.0×10^{-3} S cm^{-1}, 1.25×10^{-3} S cm^{-1} and 2.0×10^{-3} S cm^{-1} for Z8TW, Z67TW and ZMixTW, respectively. However, these values are 1.5×10^{-6} S cm^{-1}, 3.5×10^{-6} S cm^{-1}, and 2.9×10^{-6} S cm^{-1} in the case of the MMMs: PZ8TW, PZ67TW, and PZMixTW, respectively. On the other hand, we observed that the conductivity increased five or six times when the temperature change from 25 °C to 55 °C in case of MMMs but nevertheless hardly changed in the case of pure ZIFsTW. This suggests that the interaction between the ions and the polymer matrix may play an important role in determining the relationship between ionic transport and structural relaxation in terms of temperature dependence as the fillers are incorporated within the polymeric matrix.

A more quantitative analysis of the variation of the conductivity with temperature for the MMMs can be observed in Fig. 5d, in which the temperature dependence of the conductivities for the MMMs is plotted for PZ8TW, PZ67TW, and PZMixTW, respectively. From this figure, we observe an Arrhenius behavior for all the PZIFs. The activation energies values follow the trends E_{ac} (PZ67TW) = 67.8 ± 3.4 kJ/mol or 0.74 ± 0.04 eV > E_{ac} (PZ8TW) = 57.1 ± 8.1 kJ/mol or 0.59 ± 0.08 eV > E_{ac} (PZMixTW) = 13.5 ± 0.4 kJ/mol or 0.14 ± 0.03 eV.

These values are higher to those found for the activation energy of the conductivity of commercial Nafion membranes (E_a = 7 kJ/mol (0.08 eV.)) [26] and lower than those of other ZIFs [4,27], with the conductivity, in the majority of cases, being higher than or at least similar to $(NH_4)_2$ (adp) (Zn_2 (ox)$_3$·3H_2O prepared by the isothermal method [10].

Taking into account that the activation energy of our fillers is in the range between 0.13 eV in case of ZMixTW and 0.11 eV for Z8TW, we suggest that water molecules play an important role to the mechanism of proton conduction in a fashion similar to a Grotthuss mechanism, where a structure of pathways has been created into the fillers. The low values observed for the activation energies permit us thinking that these structures favor the conductivity when such fillers take part in MMMs. In this sense, the results observed for the activation energies of our MMMs have shown that the membrane of PZMixTW has an activation energy of 0.14 eV, which is around four times smaller than PZ8TW and five times than PZ67TW, respectively. This value is even smaller than that found for histamine (His@14), for which a value of 0.25 eV was estimated [4].

If we do not take into account the electrode polarization, we can observe in a complete experimental frequency range, at moderate and high frequencies in Fig. 5a–c, that the conductivity can be analyzed by means of the Jonscher law, where the real part of the conductivity is given by $\sigma'(\omega) = \sigma_{dc} + A\,\omega^n$ where A is a temperature dependent parameter and n is the power law exponent which vary but remains close to unity [28]. We can express in the high frequency region that $\sigma_{ac} = A\,\omega^n$. In this region, the dielectric permittivity is nearly independent of the frequency and tends to be a plateau, as shown in Fig. S4 for the samples Z8TW and PZ8TW.

We can see that in the high frequency region of the curves of the real part of the PZIFsTW conductivity has a tendency to increase as frequency increases. This tendency is not observed in the ZIFsTW alone. This observation permits us to conclude that polymerized samples have two regions: (1) a nearly constant loss region and (2) a super-linear power law region. Both types of ion dynamics have their origin in the confined movement of ions which should be characteristic of both ZIF type and polymer. The value of the exponent and the effect of the ZIF's concentration within the polymer matrix and temperature-dependence deserves a detailed investigation in future work.

On the other hand, the plateau in the real part of the permittivity is not observed in the case of the ZIFsTW. This is in correspondence with the non-appearance of power-law behavior in case of ZIFsTW alone.

From the results shown in Fig. 6, we can notice that all ZIFsTWs studied have dielectric spectra which show similar behavior to that of the low molecular weight ionic liquid monomers of 1-vinyl-3-pentyl imidazolium bis (trifluoromethylsulfonyl)imide (PVIM NTf_2) [25]. On the other hand, experimental observations from the dielectric response permit us conclude that for both $\frac{d\varepsilon''}{df} = 0$ and $\frac{d\sigma''}{df} = 0$ the peaks observed in the variation of the imaginary part of the conductivity and permittivity appear at the same position on the frequency axes.

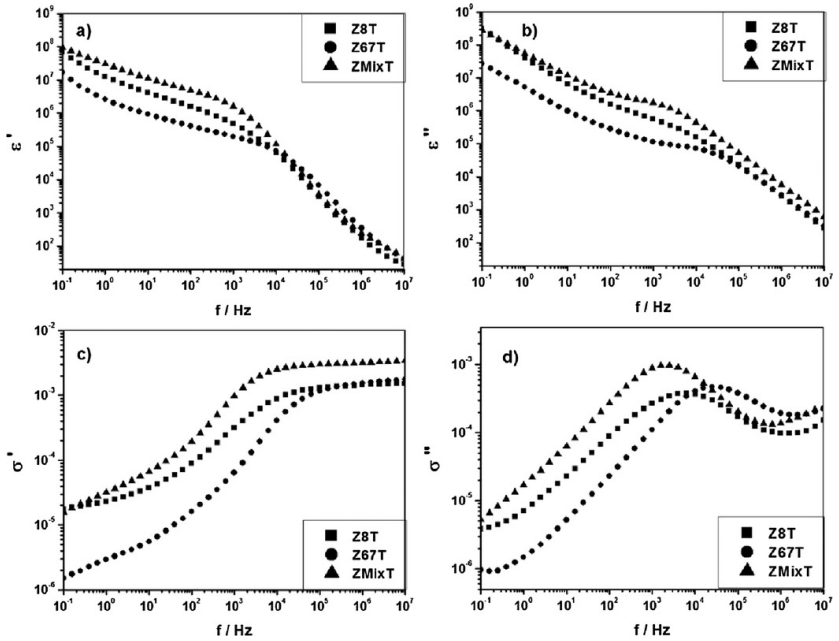

Fig. 6 Double logarithmic plot of the real and imaginary permittivity and conductivity in S cm^{-1} (ε', ε", σ' and σ") versus frequency for Z8TW, Z67TW, and ZMixTW at 55 °C.

alt-text: Fig. 6

An example of the comparison of the dielectric spectra of the ZIFsTW samples at a temperature of 55 °C is shown in Fig. 6. We noted a similar behavior for the other temperatures. A close inspection of Fig. 6c shows two clear regions which are very well-differentiated. At the high frequency region, the real part of the conductivity shows a plateau which starts at frequency f_c, where the double logarithmic plot of imaginary part of the permittivity versus frequency (Fig. 6b) exhibits a behavior of $\varepsilon'' \sim f^{-1}$ before reaching the shoulder or maximum characteristic of the full development of electrode polarization (EP). At low frequencies, the imaginary part of the permittivity again shows a linear dependence, but with a slope less than unity ($n < 1$) where the dependence of the complex permittivity shows a Debye-like shape due to an electrode polarization effect. On the other hand, from Fig. 8d we observe a minimum and a maximum in σ" for all the samples which define the "onset" and the "full development" of electrode polarization (EP) given at frequencies f_{ON} and F_{MAX}, respectively [29].

The values of the real part of the conductivity from Fig. 6c were practically the same as the values obtained from the intercept of the straight line of log ε" versus log ω when ω = 1 in the high frequency region with a slope of −1 (Fig. 6b). Therefore, these values were taken as the dc-conductivity of the samples σ_{dc}, and the values obtained for the range of temperatures from 25 °C to 75 °C for ZIFsT and 25 °C to 95 °C for PZIFsT are given in Table 3.

Table 3 Frequency values of the onset (f_{ON}) and full development of electrode polarization (f_{MAX}). Static permittivity obtained experimentally and from Eq. (5), respectively. Also, in columns six, seven, and eight, we show the dc-conductivity and frequency values obtained at electrode polarization (f_{EP}) and cut-off (f_c), which was considered the frequency at which the ac-conductivity is determined.

alt-text: Table 3

Temperature/°C	f_{MAX} ×10^{-3}/Hz	f_{ON} ×10^{-6}/Hz	ε_s (theor)	ε_s (exp)	σ_{dc} ×10^3 (S cm^{-1})	f_{EP} ×10^{-3}/Hz	f_c ×10^{-3}/Hz
Z8TW							
25	6.3	1.0	9.9	–	1.0	6.2	30.0
35	6.3	1.1	9.5	–	1.1	6.2	32.0
45	6.3	1.2	9.3	–	1.3	6.2	35.0
55	6.3	1.3	9.1	–	1.4	6.3	37.0

65	6.3	1.4	8.8	–	1.6	6.3	39.0
75	6.3	1.5	8.7	–	1.9	6.3	43.0
Z67TW							
25	25.1	1.7	16.5	–	1.1	25.1	158.0
35	24.0	2.0	13.6	–	1.2	25.2	251.0
45	25.1	2.2	12.4	–	1.3	25.2	398.0
55	25.1	2.5	10.7	–	1.4	25.2	571.0
65	35.5	3.1	10.4	–	1.6	25.2	800.0
75	63.1	4.3	10.8	–	1.8	25.3	1200.0
ZMixTW							
25	2.5	6.2	17.4	–	1.4	1.5	6.3
35	2.5	8.9	12.0	–	2.0	1.5	10.0
45	2.6	1.0	10.9	–	2.3	1.6	15.8
55	2.8	1.2	8.6	–	2.7	1.6	39.8
65	3.1	1.5	7.2	–	2.9	1.6	63.1
75	3.3	1.7	5.8	–	3.0	1.6	100.0
PZ8TW							
25	0.2	1.7	19.8	21.2	1.5	1.5	0.2
35	0.2	2.7	18.8	21.0	3.0	1.6	0.5
45	0.1	3.0	16.8	19.8	4.6	1.8	0.7
55	0.3	6.3	16.3	19.7	9.0	1.9	1.0
65	0.5	10.0	16.4	19.5	18.2	2.1	1.5
75	1.5	15.8	34.3	24.0	31.6	2.3	2.5
85	3.0	39.8	24.5	35.0	71.6	2.6	3.9
95	15.9	158.0	13.2	66.0	115.0	2.8	6.3
PZ67TW							
25	–	–	–	–	–	–	–
35	–	–	–	–	0.8	1.0	0.04
45	0.03	0.2	159.0	170.0	1.7	1.1	0.1
55	0.1	0.6	154.0	160.0	3.4	1.4	0.6

65	0.2	1.5	125.0	140.0	6.9	1.6	2.0
75	0.4	3.9	66.3	82.0	14.6	1.9	6.3
85	1.5	15.1	44.5	62.0	35.6	2.0	25.1
95	3.1	31.6	42.9	50.0	75.0	2.5	50.8
PZMixTW							
25	1.1	6.3	14.6	13.6	2.9	3.5	1.0
35	1.1	7.4	13.4	13.4	3.6	2.6	1.3
45	1.1	8.3	13.2	13.4	4.4	3.6	1.6
55	1.1	9.2	12.8	13.2	5.2	3.6	1.9
65	1.2	11.4	9.7	13.0	5.9	3.6	2.2
75	1.2	13.5	8.3	12.9	6.8	3.7	2.6
85	1.2	18.8	4.6	12.9	7.4	3.7	3.0
95	1.5	24.0	4.0	12.8	8.3	3.7	3.2

3.4.1 Determination of diffusion coefficient and ion concentration

There are a great number of alternative approaches for determining the ion mobility, the diffusion coefficient, the static permittivity, and the concentration of ionic charge under the application of an electric field [21,29–31]. Some of them use a generalization of the theory of Trukhan, following the Nernst-Planck equations which have been linearized for the dielectric dispersion caused by the electrodiffusion of ions in a polymeric membrane which are charged and confined between two electrodes [29–37]. From the analyses of the dielectric spectra of electrode polarizations, we have calculated the ion diffusivity as [33–37]

$$D = \frac{\omega_{\max}^{\tan\delta} \cdot L^2}{32(\tan\delta)_{\max,\omega}^3}. \quad \textbf{(2)}$$

where $\omega_{\max}^{\tan\delta}$ is the angular frequency corresponding to the peak in tan δ or its equivalent ε”/ε’ that represents the dielectric losses or electrical energy that is transformed into heat due to the contribution of movement of loads (ohmic losses) and mainly to the processes involved in the establishment of polarization. Notice that $(\tan\delta)_{\max,\omega}$ is the value of tan δ at $\omega_{\max}^{\tan\delta}$, and L the sample thickness. From Eq. (2), we can make an estimation of the diffusion coefficients of the samples as a function of temperature.

Fig. 7 shows the experimental values for *tan δ* as a function of the perturbation frequency for all the PZIFsT at different temperatures, (Fig. 7a: PZ8TW, Fig. 7b: PZ67TW, Fig. 7c: PZMixTW). It can be observed that the peak corresponding to the maximum *tan δ* shifts toward higher frequencies as the temperature increases. Similar plots are observed for the ZIFsT alone. Previous works from our group [32,33,35], have shown that dynamical electric double layers, described by means of Nernst-Planck-Maxwell electrodynamics, produce an excess of impedance in addition to the MWS impedance, and the combined effect of both impedances is the apparition of a maximum in *tan δ*, as the real component of the permittivity, *ε’*, rises with increasing the frequency as a reflection of the capacitance of the macropolarization that, in our case, could be due to H^+ and $N(Bu)_4^+$ ions.

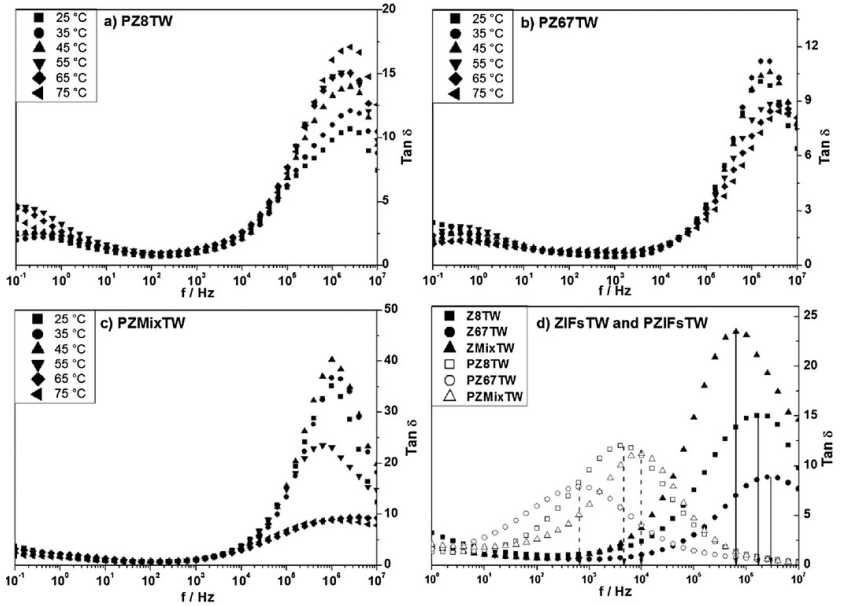

Fig. 7 Representation of tan δ vs. frequency at all temperatures for a) PZ8TW, b) PZ67TW, and c) PZMixTW. In Figure (d), we plot the tan δ vs. frequency for all the samples of ZIFsTW and PZIFsTW at 25 °C for comparison.

alt-text: Fig. 7

The dependence of the loss tangent as a function of the perturbation frequency at 25 °C of temperature for all the samples (ZIFs and PZIFs) are given in Fig. 7d. A close inspection of this plot shows that Z8TW, Z67TW and ZMixTW have values of *tan δ* higher than the PZIFsTW where the ZIFsTW has been incorporated into the polymeric matrix forming the polymerized ZIFs made up of the MMMs.

As we observed in Fig. 7, the intensity and frequency of the peaks are very sensitive to the different structural and compositions of the fillers (ZIFs), and each sample spectra generally shift to higher frequencies when the temperature increases. We can see that at 25 °C (Fig. 7d) the intensity of the peak is higher for ZMixTW (around 22 at an f_{max} of 6×10^5 Hz) than that of Z8TW (about 15 at 1.8×10^6 Hz) and Z67TW (which value is approximately 9 at 3×10^6 Hz). When we compare the polymerized ZIFs, we observe a decrease in both intensity and the frequency at the maximum. For example, PZ8TW has a t*an δ* of around 12 at 5×10^3 Hz. However, these values are 11 at 10^4 Hz for PZMixTW and 7.5 at 700 Hz in the case of PZ67TW. These values can be related to the cross-linking and number of moles of TBAH.

From the values plotted in Fig. 7 for PZIFsTW and for the ZIFsT (See the Supplementary Information), we have determined the diffusion coefficients by means of Eq. (2) for each range of temperatures. The values found in the range between 25 °C and 75 °C are plotted in Fig. 8.

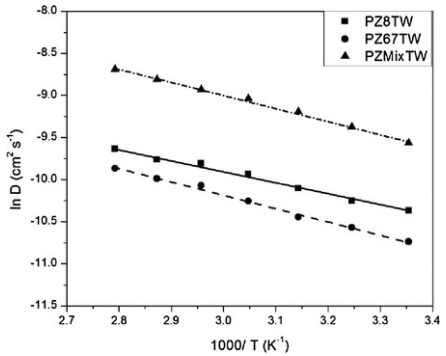

Fig. 8 Arrhenius plot for the diffusion coefficients obtained according to Eq. (2) for the ZIFsTW and PZIFsTW studied.

alt-text: Fig. 8

From Fig. 8, we can obtain the activation energy associated with the ions $[N(Bu)_4]^+$ transported in the membranes. The values calculated from the slopes are 11.0 ± 0.1 kJ/mol, 12.8 ± 0.2 kJ/mol, and 13.2 ± 0.1 kJ/mol, for P8TW, P67TW, and PMixTW, respectively. These quantities are slightly higher than the activation energy reported for Nafion-117 membranes and perfluorinated membranes doped with polyaniline [37,38]. On the other hand, from the experimental values for *tan δ* as a function of the perturbation frequency for all of the temperature ranges such as those shown in Fig. 7 for PZIFsTW and the known thickness of the samples, L, the inverse of Debye length, κ, can be estimated according to the following equation [33,37]:

$$(\tan\ \delta)_{\max,\omega} \approx \sqrt{\frac{\kappa L}{8}} \quad \textbf{(3)}$$

Notice that the Eq. (3) is only valid in the case that $\kappa L >> 1$. From this expression we can calculate the values of parameter κL for each sample and temperature. In our MMMs the inverse of Debye length follows the trend κ(PZ8TW) < κ(PZ67TW) < κ(PZMixTW) at 25 °C, varying from about of 8.5×10^{-7} m^{-1} for PZ8TW to 2.6×10^{-5} m^{-1} in the case of PZMixTW.

Obtaining the true contribution of each ion to the ionic transport in polymerized MMMs is very difficult. For this, it is necessary to know the respective roles of the cations and anions in the samples from conductivity measurements. As the conductivity is obtained for the complete system, it represents the sum of the total contributions of the mobile charges, i.e., $\sigma_{dc} = \sigma_+ + \sigma_-$ [25]. Thus, although all the available charges participate in the ionic transport, it can be assumed that the highest plausible contribution to the true conductivity, $\sigma = \sigma_{dc}$, for all the samples is only associated with the mobility of the cations or assumed for the case in which both cations and anions have equal diffusion coefficients. In such cases, we express in a first approximation that conductivity and diffusivity are related as [33,36]

$$\sigma_{dc} = \epsilon_s \epsilon_0 \kappa^2 \frac{D_+}{2} \quad \textbf{(4)}$$

When the values of the inverse Debye length can be obtained from the peaks of the loss tangent, the values of ε_s can be estimated. Eq. (4) provides an indirect method to calculate the static permittivity, ε_s. This method can be compared with the equation of Anatoly Serguei [39], where the permittivity can be expressed in function of the values f_{ON} and f_{Max} found from the curves of double logarithmic plot of σ" versus frequency, as

$$\varepsilon_s = \frac{\sigma_{dc}}{2\pi\varepsilon_0} \frac{f_{Max}}{f_{ON}^2} \quad \textbf{(5)}$$

Fig. 9 show the curves of double logarithmic plot of σ" versus frequency in the complete range of temperatures studied for PZ8TW, PZ67TW and PZMixTW. From this figure, we have determined for each sample at each temperature the frequency values of the onset (f_{ON}) and full development of electrode polarization (f_{MAX}), respectively, which permits us obtain the static permittivity following Eq. (5). The mean values obtained following the two procedures are gathered in Table 2 as ε_s theoretical. Also, for comparison, we have tabulated the values observed from the experimental plots of ε' versus frequency for all the samples (ZIFs and MMMs), as ε_s experimental. Comparison of both results notes the excellent agreement between the static permittivity values obtained theoretically following Eqs. (4) and (5), respectively, with respect to the experimental ones. A close inspection of these results indicates that ε_s decreases when the temperature increases, the values obtained for the ZIFs are smaller than those of the PZIFs, and both are in good agreement with the values found experimentally.

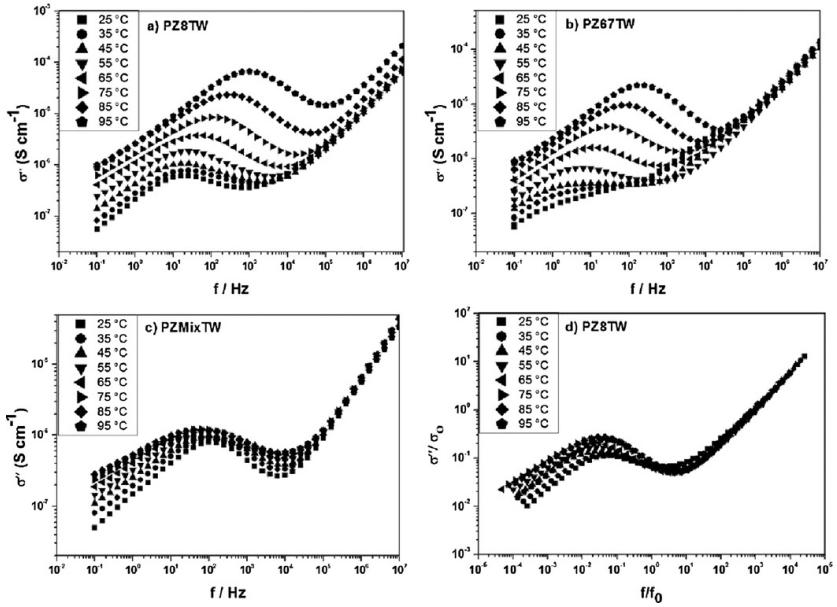

Fig. 9 (a), (b), and (c) are the double logarithmic plots of the imaginary parts of the conductivity vs. frequency for each of the PZIFsTW. (d) Master curve of the normalized plots respect to the imaginary part of the conductivity for PZ8TW.

alt-text: Fig. 9

Fig. 9d shows a description of the correspondence between the time/frequency and temperature for conductivity using the scaling ansatz [40], where log (σ'/σ_{dc}) scale with log (f/f_c), where f_c is the frequency marking the onset of the dc-conductivity. This result has shown that the scaling function is also perfectly applicable to MMMs. We have observed similar results for the imaginary components of the conductivity, ε' and ε", indicating that the dielectric and conductivity measurements scale perfectly with the frequency upon varying the temperature. The experimental measurements obtained for all the ZIFs and MMMs respect to the permittivity (ε' and ε") and conductivity (σ' and σ") collapse onto a single chart when normalized. All charts collapse into one if scaled with respect to f_c. This suggests an identical thermal activation of charge transport and electrode polarization.

Neglecting ion-ion interactions, the dc-conductivity can be expressed as $\sigma_{dc} = n\ q\ \mu$, where q is the elemental charge, n the number density of charge carriers, and μ is the mobility related with the diffusivity according to the Einstein relation by $\mu = q\ D/kT$, where D is the ionic diffusion coefficient and kT the thermal energy. Finally, the free-ion density can be obtained combining the relations of the dc-conductivity and the ionic mobility as:

$$n = \frac{kT \cdot \sigma_{dc}}{q^2 D} \quad \textbf{(6)}$$

Eq. (6), given by Wang and co-workers [36], allowed for the determination of the average density of charge carriers from the previously-determined values of the ionic conductivity (Table 3) and from the values of diffusion coefficients calculated according to Eq. (2) (Fig. 7). Assuming the electrolyte is univalent, we have estimated the values of the charge density for each one of the polymerized samples (PZIFsTW) as a function of 1000/T, as is shown in Fig. 10. A close inspection of Fig. 10 shows that the free ion density decreased at lower temperatures for PZ8TW and PZ67TW. However, it is practically constant in the case of PZMixTW. Guest molecules concentration within the fillers appears to be a determining factor of the charge carrier density. Characteristic local electric anisotropies for each filler governs the different amounts of doping with TBAH through attractive interactions that confine varying amounts of TBAH electrolyte.

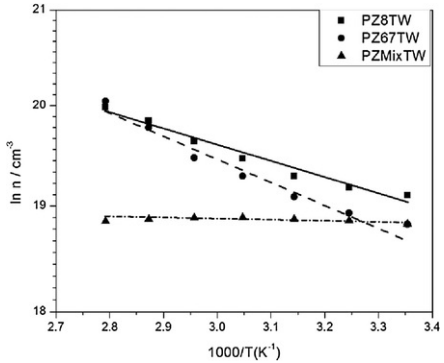

Fig. 10 Temperature dependence of free ion number density (n) for the samples PZIFTW. These values have been calculated from the electrode polarization effect using the generalized Trukhan model described previously in the literature [29,36].

alt-text: Fig. 10

From the Arrhenius fit in Fig. 10, we have estimated the dissociation energy. The values found for the PZIFsTW are 0.14 ± 0.02 eV for PZ8TW, 0.20 ± 0.03 eV in the case of PZ67TW, and 0.0040 ± 0.0004 eV for PZMixTW. We can observe that the dissociation energy is 50 times higher for PZ67TW than for PZMixTW and 35 times higher in the case of PZ8TW. These values are restricted to the assumption of Arrhenius behavior given for the PZ676TW and PZ8TW because this type of demeanor is not clear for all the range of temperatures studied.

Fig. 11 plots the dc-conductivity versus the characteristic frequency, ω_c, for each of the samples. From this figure, we saw that the Barton-Nakajima-Namikawa (BNN) relation is satisfied and subsequently suggested that the conduction and dielectric relaxation have their origins in a single diffusion process. On the basis of the agreement between ω_c ($\omega_c = 2\pi f_c$) and the structural relaxation rate of our MMM samples, we can conclude that the incorporation of the ZIFs doped with tetrabutylammonium hydroxide into the polymeric matrix enhances the charge transport in the membranes of the matrix mixture studied. This suggests that the interaction between the ions $[N(Bu)_4]^+$ and the polymeric matrix of PEI may play an important role in determining the coupling between the charge transport and structural relaxation of PEI for each temperature. On the other hand, from the slopes shown in Fig. 9, we can conclude that the strongest interaction is observed for the sample PZ8TW and the trends follow the sequence PZ8TW > PZMixTW > PZ67TW.

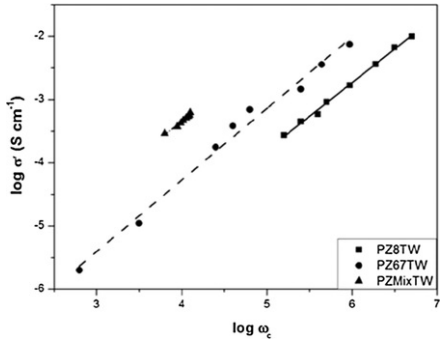

Fig. 11 Dc-conductivity versus the characteristic rates of charge transport ω_c for the different PZIFsTW.

alt-text: Fig. 11

4 Conclusions

The combination of the thermogravimetric curve with thermal treatment and spectroscopic analysis allows us to conclude that for each imidazole ring in Z8T and Z67T, there are similar amounts of tetrabutylammonium hydroxide $[(C_4H_9)_4N^+OH^-]$ entities and water molecules while there is more than twofold that amount of the same entity in ZMixT.

Half a TBAH unit per ZIF formula unit allowed water association at 5.7% in the Z8T and Z67T ZIF structures while 1.35 TBAH units per ZIF formula unit leaves less space for water association, which is decreased to 4.6% as determined by TG analysis. Z8T and Z67T frameworks show a small difference in water and TBAH content within the set of temperatures studied due to their uniform electrical nature. These results highlight the fact that local charge

anisotropy in ZMixT accommodates the TBAH electrolyte to travel and to accumulate within the ZMix better than Z8 and Z67. By doing so, it also favors proton transport as discussed in this work.

The charge transport mechanism in ZIFs and PZIFs has been analyzed in detail through dielectric spectroscopy using the electrode polarization model. The theoretical approach perfectly reproduces the scaling laws.

From the experimental data of the dc-conductivity we have probed the consistency of the Anatoly-Sherguei (A. Serghei, 2009)(A. Serghei, 2009)(A. Serghei, 2009) equation $\varepsilon_s = \frac{\sigma_{dc}}{2\pi\varepsilon_0} \frac{f_{Max}}{f_{ON}^2}$ for the determination of the static permittivity for Z8TW, Z67TW, ZMixTW, and its MMM obtained on polyether imide films.

We observed an overestimate of ion diffusivity, which may be related to the model of electrode polarization used in its determination. The diffusivities estimated at 25 °C are 3.1 × 10^{-5} cm^2 s^{-1}, 2.2 × 10^{-5} cm^2 s^{-1}, and 7.0 × 10^{-5} cm^2 s^{-1} for PZ8TW, PZ67TW, and PZMixTW, respectively.

From the analysis of the free-ion number density we have estimated that the dissociation energy is 50 times higher for PZ67TW than that of PZMixTW and 35 times higher in the case of PZ8TW. These values can be related with an overestimation of ion diffusivity. These results can be attributed to the electrode polarization analysis of ionic mobility.

Acknowledgements

This research has been supported by the ENE/2015-69203-R project, granted by the Ministerio de Economía y Competitividad (MINECO), Spain, and grants from National Mexican Council for Science and Technology for the scholarships of Ph.D. No. 356825 and mixed scholarship 2015 – MZO2016-mobility in the foreigner granted to Jesus Vega Moreno registered scholarship holder number 256015. Thanks to the CONACYT Program for the fellowship at the Universidad Politécnica de Valencia (UPV) and Universitat Jaume ~~that~~ I that PhD student Jesús Vega used to carry out the experimental studies of this work. DGAPA-PAPIIT IG-100315.

We would like to thank to Prof. Dr. Santiago V. Luis for the support received in the preparation of the materials and his comments made on the discussion in the study of the characterizations made by DRX, FT-IR and SEM, Dr. Jose Antonio Irán Díaz Góngora for supporting the student's stay, and Alberto López Vivas and Raúl Reyes Ortíz for their technical assistance.

References

[1] I. Dincer and M. Rosen, Sustainability aspects of hydrogen and fuel cell systems, *Energy for Sustainable Development* **15**, 2011, 137.

[2] E. Bakangura, L. Wu, L. Ge, Z. Yang and T. Xu, Mixed Matrix Proton Exchange Membranes for Fuel Cells: State of the Art and Perspectives, *Progress in Polymer Science* **57**, 2016, 103.

[3] J.H. Kim, S.K. Kim, K. Namb and D.W. Kim, Composite proton conducting membranes based on Nafion and sulfonated SiO_2 nanoparticles, *Journal of Membrane Science* **415**, 2012, 696.

[4] M. Yoon, K. Suh, S. Natarajan and K. Kim, Proton Conduction in Metal–Organic Frameworks and Related Modularly Built Porous Solids, *Angew. Chem. Int. Ed* **52**, 2013, 2688.

[5] A. Iulianelli and A. Basile, Sulfonated PEEK-based polymers in PEMFC and DMFC applications: A review, *International Journal of Hydrogen Energy* **37**, 2012, 15241.

[6] L. Li, J. Zhang and Y. Wang, Sulfonated poly (ether ether ketone) membranes for direct methanol fuel cell, *Journal of Membrane Science* **226**, 2003, 159.

[7] G. Xiaomin, Liu Yonghua and Li Jinlong, Review on Modification of Sulfonated Poly (ether-ether-ketone) Membranes Used as Proton Exchange Membranes, *Materials Science* **21** (4), 2015.

[8] S. Mollá and V. Compañ, Nanocomposites SPEEK-based membranes for Duirect Methanol Fuel Cells at intermediate temperatures, *J. Membr. Sci.* **492**, 2015, 123.

[9] S.P. Nunes, B. Ruffmann, E. Rikowski, S. Vetter and K. Richau, Inorganic modification of proton conductive polymer membranes for direct methanol fuel cells, *Journal of Membrane Science* **203**, 2002, 215.

[10] M. Sadakiyo, T. Yamada and H. Kitagawa, Rational Designs for Highly Proton-Conductive Metal-Organic Frameworks, *J. Am. Chem. Soc.* **131**, 2009, 9906.

[11] M. Sadakiyo, H. Kasai, K. Kato, M. Takata and M. Yamauchi, Design and Synthesis of Hydroxide Ion-Conductive Metal-Organic Frameworks Based on Salt Inclusion, *J. Am. Chem. Soc.* **136**, 2014, 1702.

[12] C. McCarthy, V. Guerrero, G. Barnett and H. Jeong, Synthesis of Zeolitic Imidazolate Framework Films and Membranes with Controlled Microstructures, *Langmuir* **26**, 2010, 14636.

[13] K.Y.A. Lin and H.A. Chang, Ultra-High Adsorption Capacity of Zeolitic Imidazole Framework-67 (ZIF-67) for Removal of Malachite Green From Water, *Chemosphere* **139**, 2015, 624.

[14] J.B. James and Y.S. Lin, Kinetics of ZIF-8 Thermal Decomposition in Inert, Oxidizing, and Reducing Environments, *J. Phys. Chem. C* **120**, 2016, 14015.

[15] A. Samano, R. Cabrera, J. Hernández, A.A. Lemus and E. Reguera, Separation of H_2–CO_2 and CH_4-CO_2 binary mixtures by zeolite-like imidazolate frameworks, *Surfaces and Interfaces* **5**, 2016, 55.

[16] K.S. Park, Z. Ni, A.P. Cote, J.Y. Choi, R. Huang, F.J. Uribe, H.K. Chae, M. ŐKeeffe and O.M. Yaghi, Exceptional chemical and thermal stability of zeolitic imidazolate frameworks, *PNAS* **103** (27), 2006, 10186.

[17] R. Banerjee, A. Phan, B. Wang, C. Knobler and O.M. Yaghi, High-throughput synthesis of zeolitic imidazolate frameworks and application to CO_2 capture, *Science* **319**, 2008, 939.

[18] K. Zhang, L. Zhang and J. Jiang, Adsorption of C1–C4 Alcohols in Zeolitic Imidazolate Framework-8: Effects of Force Fields, Atomic Charges, and Framework Flexibility, *J. Phys. Chem. C* **117**, 2013, 25628.

[19] K.S.W. Sing, D.H. Everett, R. Haul and I. Moscou, Reporting physisorption data for gas/solid systems, *Pure and appl.chem.* **54**, 1982, 2201.

[20] C. Krause, J.R. Sangoro, C. Iacob and F. Kremer, Charge Transport and Dipolar Relaxations in Imidazolium-Based Ionic Liquids, *J. Phys. Chem B.* **114**, 2010, 382.

[21] J. Klein, S. Zhang, S. Dou, B.H. Jones, R. Colby and J. Runt, Modeling electrode polarization in dielectric spectroscopy: Ion mobility and mobile ion concentration of single-ion polymer electrolytes, *J. Chem Phys.* **124**, 2006, 144903.

[22] S. Tominaka and A.K. Cheetham, Intrinsic and extrinsic proton conductivity in metal-organic frameworks, *RSC Advances* **4**, 2014, 54382.

[23] C. Serre, F. Millange, C. Thouvenot, M. Noguès, G. Marsolier, D. Louër and G. Férey, Very Large Breathing Effect in the First Nanoporous Chromium(III)-Based Solids: MIL-53 or $Cr^{III}(OH)\cdot\{O_2C\text{-}C_6H_4\text{-}CO_2\}\cdot\{HO_2C\text{-}C_6H_4\text{-}CO_2H\}_x\cdot H_2O_y$, *J. Am. Chem. Soc.* **124** (45), 2002, 13519.

[24] A. Comotti, S. Bracco, P. Sozzani, S. Horike, R. Matsuda, J. Chen, M. Takata, Y. Kubota and S. Kitagawa, Nanochannels of Two Distinct Cross-Sections in a Porous Al-Based Coordination Polymer, *J. Am. Chem. Soc.* **130**, 2008, 13664.

[25] J.R. Sangoro, C. Iacob, A.L. Agapov, Y. Wang, S. Berdzinski and H. Rexhausen, Decoupling of ionic conductivity from structural dynamics in polymerized ionic liquids, *Soft Matte* **10**, 2014, 3536.

[26] S. Molla and V. Compañ, Polyvinyl alcohol nanofiber reinforced Nafion membranes for fuel cell applications, *J. Membr. Sci.* **372**, 2011, 191.

[27] B.R. Matos, C.A. Goulart, E.I. Santiago and Muccillo, Proton conductivity of perfluorosulfonate ionomers at high temperature and high, *Applied physics letters* **104**, 2014, 091904.

[28] A.K. Jonscher, A new understanding of the dielectric relaxation of solids, *J. Materials Science.* **16**, 1981, 2037.

[29] Y. Wang, C.N. Sun, F. Fan, J.R. Sangoro, M.B. Berman, S.G. Greenbaum, T.A. Zawodzinski and A.P. Sokolov, Examination of methods to determine free-ion diffusivity and number density from analysis of electrode polarization, *Physical Review, E* **87**, 2013, 042308.

[30] R. Coelho, Sur la relaxation d'une charge d’espace, *Revue Phys. Appl.* **18**, 1983, 137.

[31] J.R. MacDonald, Theory of ac Space-Charge Polarization Effects in Photoconductors, Semiconductors, and Electrolytes, *Phys rev.* **92**, 1953, 4.

[32] A. Munar, A. Andrio, R. Iserte and V. Compañ, Ionic conductivity and diffusion coefficients of lithium salt polymer electrolytes measured with dielectric spectroscopy, *Journal Non-Crystalline solids* **357**, 2011, 3064.

[33] T.S. Sorensen, V. Compañ and R. Díaz, Complex permittivity of a film of poly [4-(acryloxy)phenyl-(4-chlorophenyl)methanone] containing free ion impurities and the separation of the contributions from interfacial polarization, Maxwell-Wagner-Sillars effects and dielectric relaxations, *J. Chem Soc.* **92**, 1996, 1947.

[34] V. Compañ, R. Diaz and E. Riande, Diffusion coefficients of conductive ions in a copolymer of vinylidene cyanide and vinyl acetate obtained from dielectric measurements using the model of Trukhan, *J. Applied Physics.* **79**, 1996, 403.

[35] Y. Wang, F. Fan, A.L. Agapov, T. Saito, J. Yang, X. Yu, K. Hong, J. Mays and A.P. Sokolov, Examination of the fundamental relation between ionic transport and segmental relaxation in polymer electrolytes, *Polymer* **55**, 2014, 4067.

[36] T.S. Sorensen and V. Compañ, Complex Permittivity of a Conducting, Dielectric Layer containing Arbitrary Binary Nernst-Planck Electrolytes with Applications to Polymer Films and Cellulose Acetate Membranes, *J. Chem Soc. Faraday Trans.* **91**, 1995, 4235.

[37] A. Munar, K. Suarez, O. Solorza, N.P. Berezina and V. Compañ, Performance of Hydrogen Fuel Cell MEAs Based on Perfluorinated Nanocomposite Membranes Modified by Polyaniline, *Journal of The Electrochemical*

Society **157**, 2010, B1186.

[38] T.A. Zawoddzinsk, M. Neeman, I.O. Sillerud and S. Gottesfeld, *J. Phys. Chem.* **95**, 1991, 6040.

[39] A. Serghei, M. Tress, J.R. Sangoro and F. Kremer, Electrode polarization and charge transport at solid interfaces, *Phys. Rev B* **80**, 2009, 184301.

[40] R. Murugaraj, AC conductivity and its scaling behavior in borate and bismuthate glasses, *J. Mater. Sci.* **42**, 2007, 10065.

Graphical abstract

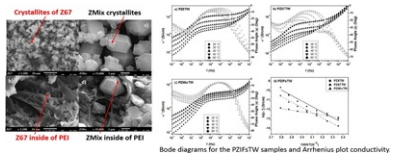

Bode diagrams for the PZIFsTW samples and Arrhenius plot conductivity.

Highlights

- The ionic pair of tetrabutylammonium hydroxide was introduced within the Z8, Z67 and ZMix.
- Mixed matrix membrane of PEI/ZIFsT prepared using the modified ZIFs as fillers have been characterized.
- The relative amount of host molecules in Z8, Z67 and ZMix was determined.
- The local electric anisotropy characteristic of ZMix favors the amount of doping the TBAH salt.
- Activation energies for ZMixTW fillers and PZMixTW membranes were 0.13 and 0.14 eV, respectively.

Queries and Answers

Query: The author names have been tagged as given names and surnames (surnames are highlighted in teal color). Please confirm if they have been identified correctly.
Answer: Yes

Query: Please check the presentation of all affiliations for correctness.
Answer: All the affiliations are correct, but if is possible change Física aplicada by Física Aplicada

Query: Please check the designated corresponding author e-mail address, and correct if necessary.
Answer: The corresponding author and e-mail address are correct

Query: “Your article is registered as a regular item and is being processed for inclusion in a regular issue of the journal. If this is NOT correct and your article belongs to a Special Issue/Collection please contact a.elumalai@elsevier.com immediately prior to returning your corrections.”
Answer: OKEY. The article is registered as a regular item and should be processed for inclusion in a regular issue of the journal.

Query: Please check the hierarchy of section headings.
Answer: Is correct.

Query: Please note that Supplementary Figs. are cited in the text but not provided. Please provide Supplementary information or delete the citations from the text.

Answer: In attached file we have included the supplementary information. I thought it was saved from the previous version and did not need to re-include it

Query: One or more sponsor names and the sponsor country identifier may have been edited to a standard format that enables better searching and identification of your article. Please check and correct if necessary.

Answer: All the sponsor names and country identifications are correct.

Query: Please check the presentation of Tables 1 and 3, and correct if necessary.

Answer: Please, If it is possible to place the values in the columns of the tables 1, 2 and 3 in a centered way. (See files attached.